electronics

MDPI

Communication

An In-Band Low-Radar Cross Section Microstrip Patch Antenna Based on a Phase Control Metasurface

Fang Li [1], Miao Lv [1,*], Min Wang [1] and Yongtao Jia [2]

[1] The 20th Research Institute of China Electronics Technology Group Corporation, Xi'an 710068, China; kleelf@163.com (F.L.); godspeed8851@163.com (M.W.)
[2] The Key Laboratory of Antennas and Microwave Technology, Xidian University, Xi'an 710071, China; jiazong0629@163.com
* Correspondence: antenna_lv@126.com

Abstract: An in-band low radar cross section (RCS) microstrip patch antenna based on a phase control metasurface is proposed. As the size of the phase control metasurface changes, it will have different phase adjustments to the incident electromagnetic wave. Two kinds of phase control metasurfaces with a 90° reflection phase difference are arranged in a checkerboard configuration and loaded above a microstrip array antenna. The metal of the microstrip array antenna can fully reflect the electromagnetic wave, so the incident wave passes through the metasurface again and forms a reflected wave with a phase difference of 180° ± 37° when passing through the phase control metasurfaces of different sizes. Thus, the microstrip array antenna can achieve in-band RCS reduction. The metamaterial forms a transmission window in the microstrip patch array antenna band to maintain the radiation performance. Finally, a reasonable agreement is obtained between the measured and simulated results.

Keywords: radar cross section (RCS); phase control metasurface; microstrip patch antenna

Citation: Li, F.; Lv, M.; Wang, M.; Jia, Y. An In-Band Low-Radar Cross Section Microstrip Patch Antenna Based on a Phase Control Metasurface. *Electronics* **2024**, *13*, 1718. https://doi.org/10.3390/electronics13091718

Academic Editor: Ikmo Park

Received: 7 April 2024
Revised: 22 April 2024
Accepted: 26 April 2024
Published: 29 April 2024

1. Introduction

Modern warfare is electronic warfare carried out through radar systems. The search and tracking capabilities of related equipment in war have been greatly improved, which has a significant impact on the survival and combat capabilities of traditional weapon systems in war. The traditional radar cross section (RCS) reduction methods include modification technology [1,2] and radar absorbing materials [3–5]. However, these methods have an impact on the antenna's radiation performance.

In recent years, electromagnetic metamaterials have been utilized to realize RCS reduction in antennas, such as artificial magnetic conductors (AMCs), polarization conversion metasurface (PCM), resistive metasurface, and frequency selective rasorber (FSR). In [6], two different AMC structures on a checkerboard around the microstrip antenna are proposed, redirecting the scattering waves of the microstrip antenna from 8.8 GHz to 17.3 GHz. Furthermore, in [7], the AMC is placed beneath the path of the microstrip antenna, enabling RCS reduction from 5.8 GHz to 21.5 GHz. In [8], a garland-shaped dual-band PCM is proposed, and its checkerboard arrangement around the microstrip antenna suppresses the backward scattering waves. However, the expanding the size of the antenna floor with an AMC and PCM is not suitable for reducing the RCS of the microstrip patch array antenna. In [9], the antenna realizes out-of-band RCS reduction by PCM above the slot array. The RCS reduction in the antenna has also been realized by absorbing the incident waves. In [10], a resistive metasurface is loaded on top of an array antenna to absorb out-of-band incident electromagnetic waves from the array antenna, but it causes a decrease in gain. In [11], the frequency selective rasorber (FSR) is loaded above the array antenna. Electromagnetic waves within the operating frequency band of the antenna pass through the FSR normally, while waves outside the band are absorbed by the resistance to reduce the RCS.

However, due to the periodicity of metamaterials, the lateral size of the overall antenna can be too large. In [12], an anisotropic resistive metasurface was proposed and applied to the RCS reduction in microstrip antennas. The metasurface can absorb the cross-polarized incident waves and transmit the co-polarization electric waves in the operating frequency band, enabling the cross-polarized RCS reduction and the low gain loss. Therefore, in-band co-polarized RCS reduction is hardly realized.

In order to overcome the above problems, a phase control metasurface is proposed to realize the in-band RCS reduction in the antenna according to the phase cancellation theory in this paper. The operating frequency band of the microstrip patch antenna is 9.2–9.8 GHz and in the whole operating frequency band, the reduction in the co-polarized RCS is greater than 10 dB, and the reduction in the cross-polarized RCS is greater than 9.1 dB. The remainder of this article is organized into three sections. Section 2 presents the design process and analysis of the in-band low-RCS antenna. In Section 3, an analysis of the measured results is provided. Finally, Section 4 offers a summary.

2. Low-RCS Array Antenna Design

2.1. Mechanism of Phase Control Metasurface

Due to the difference between the radiation and scattered wave paths of the antenna, by applying distinct control factors to both the radiated and scattered electromagnetic waves, a different control of the antenna radiation and scattering can be achieved. Specifically, when the electromagnetic wave passes through the metasurface, reaches the antenna, and then passes through the metasurface again, it undergoes an additional metasurface reflection and phase modulation compared to the radiated electromagnetic wave. In order to ensure the radiation performance and scattering performance of the antenna at the same time, the phase control unit must possess excellent transmission properties. That is, in the operating frequency band, the electromagnetic wave must pass through the metamaterial with as little loss as possible, and at the same time, it must have a sufficient transmission phase. The RCS formula for two parameter-size phase control metasurfaces is:

$$\text{RCS reduction} = 10\log\left|\frac{A_1 e^{P_1} + A_2 e^{P_2}}{2}\right| \quad (1)$$

where A_1 and A_2 represent the reflection amplitudes of the two different-sized phase control metasurfaces, and P_1 and P_2 are the reflection phases of metasurfaces.

The existence of the antenna metal floor means that the reflection amplitude is approximately equal to 1. The calculations show that when $|P_1 - P_2| = 180 \pm 37°$, the RCS reduction amount reaches 10 dB. Since the incident electromagnetic wave passes through the metasurface twice, the metasurface unit must have a transmission phase of about 90° while the transmission amplitude is close to 0.

2.2. Antenna Unit Design

Figure 1 shows the structure of the phase control metasurface unit. The substrate has a relative permittivity of 3.66, and the upper patch consists of two rectangular boxes. The unit period P = 7.5 mm, the thickness t = 1 mm, the width of the rectangular frame w = 0.1 mm, and the distance d = 4.2 mm. The unit performance at 9.65 GHz is analyzed in detail. For the plane wave incident with x-polarization, as shown in Figure 2, when the other parameters remain unchanged except the size of the inner rectangular frame L changing from 4 mm to 4.9 mm, the transmission amplitude remains close to zero, while the transmission phase experiences a consistent shift. Due to the symmetry of the cell, the performances of the unit for y-polarization are the same as those for x-polarization. It can be seen that when the size of the inner rectangular frame is changed from 4 mm to 4.9 mm, the metasurfaces of both sizes have a transmission phase difference of 90°. Then, the phase control metasurface is loaded on top of a metal reflector. As Figure 3 illustrates, varying the size of the inner rectangular frame from 4 mm to 4.9 mm results in a reflection phase

difference of both x-polarization and y-polarization being within 180° ± 37°, while the reflection amplitude remains relatively unchanged.

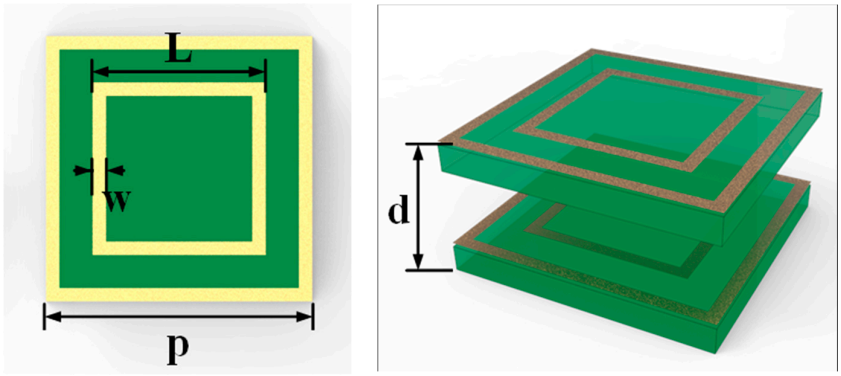

(**a**) (**b**)

Figure 1. Structure of the metasurface unit. (**a**) Top view of unit; (**b**) side view of unit.

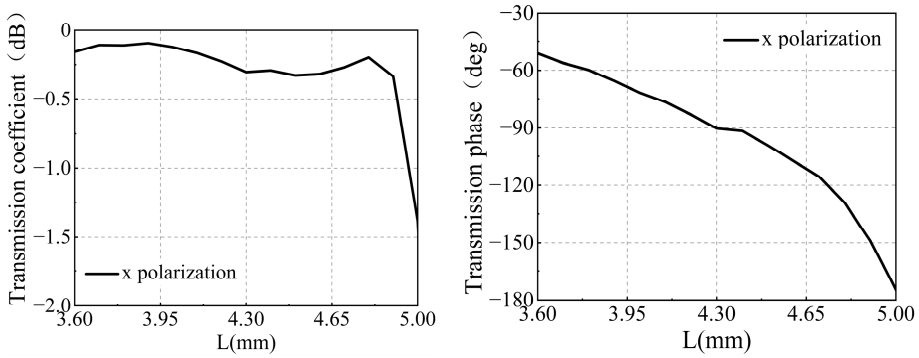

(**a**) (**b**)

Figure 2. The simulated transmission performance of the metasurface unit. (**a**) Transmission coefficient; (**b**) transmission phase.

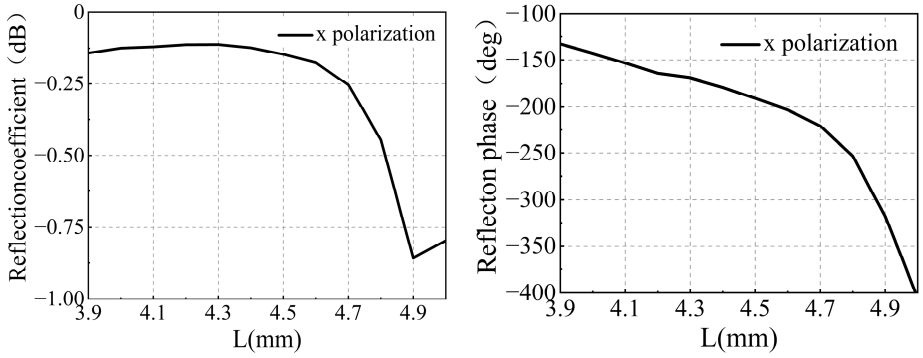

(**a**) (**b**)

Figure 3. Simulation results of a metasurface unit loaded with a metal plate. (**a**) Transmission coefficient. (**b**) Transmission phase.

In order to ensure that the electromagnetic waves can be radiated normally through the metasurface when the antenna is working, a microstrip patch antenna unit at the same working frequency as the phase control metasurface is designed. The microstrip patch unit has a period of $1/2\lambda_0$, whereas the phase control unit has a period of $1/4\lambda_0$. The designed phase control unit is arranged in a 2 × 2 array configuration and mounted above the microstrip patch unit. The overall structure is shown in Figure 4. The microstrip

antenna unit features a dielectric substrate made of Arlon Ad450, with parameters including a = 8.4 mm, b = 6.7 mm, and c = 2.9 mm.

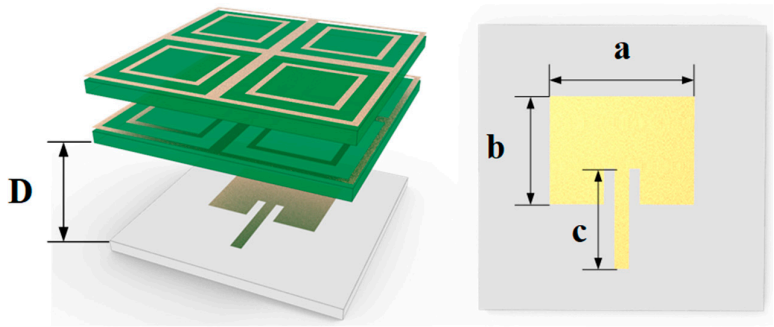

Figure 4. Antenna unit structure loaded with phase control metasurface. (**a**) 3D view of the whole antenna unit structure; (**b**) top view of the microstrip antenna.

The overall unit simulation results for x-polarized and y-polarized incident waves are shown in Figure 5. For the x-polarized incident wave, when L varies from 4 mm to 4.9 mm, the reflection amplitude varies by 0.45 dB, and the phase shifts by 210°. Similarly, for the y-polarized incident wave, as L changes from 4 mm to 4.9 mm, the reflection amplitude differs by 0.45 dB, and the phase changes by 155°. Evidently, both the x-polarization and y-polarization of the antenna unit meet the RCS reduction condition, which requires a phase difference of 180° ± 37° and a relatively stable reflection amplitude within a certain range. Figure 6 demonstrates the simulation results of the radiation pattern. When the loaded phase control metasurface has a length L of 4 mm, compared to the microstrip patch antenna unit, there is no decrease in the gain of the designed antenna unit and the pattern hardly changes. When L is 4.9 mm, the main lobe of the designed unit narrows, but the gain increases by 1.44 dB.

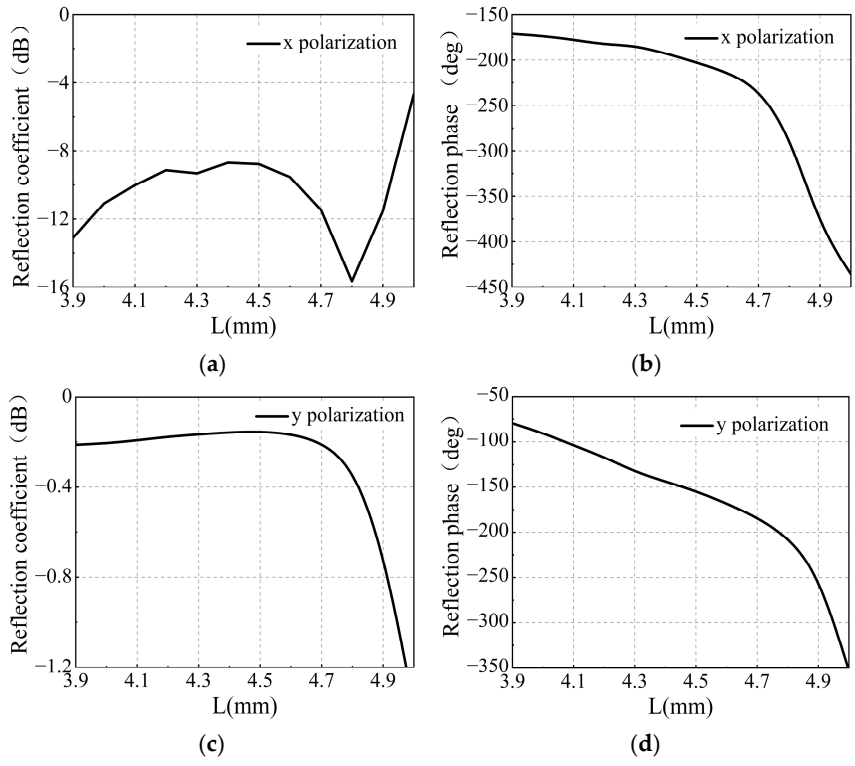

Figure 5. Simulation results. (**a**) x-polarization reflection coefficient; (**b**) x-polarization reflection phase; (**c**) y-polarization reflection coefficient; (**d**) y-polarization reflection phase.

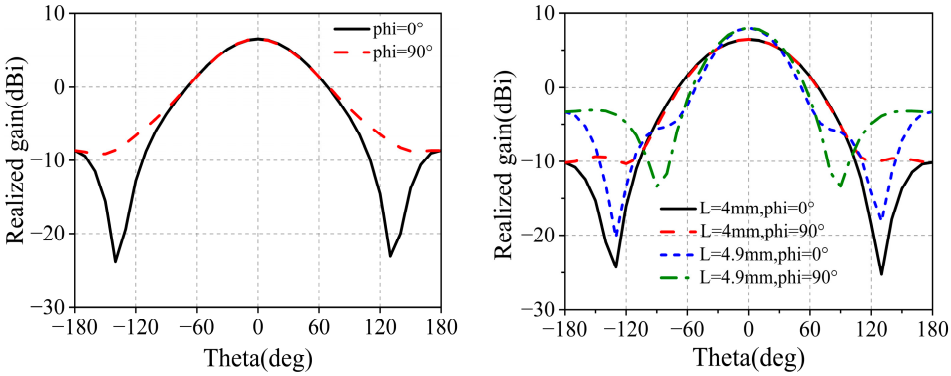

Figure 6. Simulation results: (**a**) Microstrip antenna unit; (**b**) microstrip antenna unit loaded with metasurface.

2.3. Structures of the Proposed in-band Low-RCS Microstrip Antenna

The antenna units of two sizes are arranged in a checkerboard pattern. A one-to-sixteen power divider with equal power and different phases is designed. The unequal-phase power divider can compensate for the radiation phases of the antenna units, ensuring that the radiation performance of the designed antenna remains unaffected. The reference array antenna and the designed antenna structures are depicted in Figure 7. The reference antenna measures the total size of 61 mm × 61 mm × 1 mm and distance between the antenna units of D = 4 mm, with other unchanged dimensions compared with the reference antenna. The bends indicated by red circles in Figure 7a serve to ensure unequal-phase feeding to the two types of phase-regulating metasurface modules. Figure 8 illustrates that the phase value is approximately 50° to compensate for the phase difference of the radiation waves for two antenna units. Figure 9 compares the simulation results of the designed and reference antennas. Upon loading the phase control metasurface, the patch array antenna still operates at 9.65 GHz, with the peak value remaining virtually unchanged or experiencing a slight increase. Figure 10 displays the radiation patterns of the designed and reference antennas operating at 9.65 GHz. Notably, the metasurface has minimal impact on the radiation pattern of the microstrip array antenna.

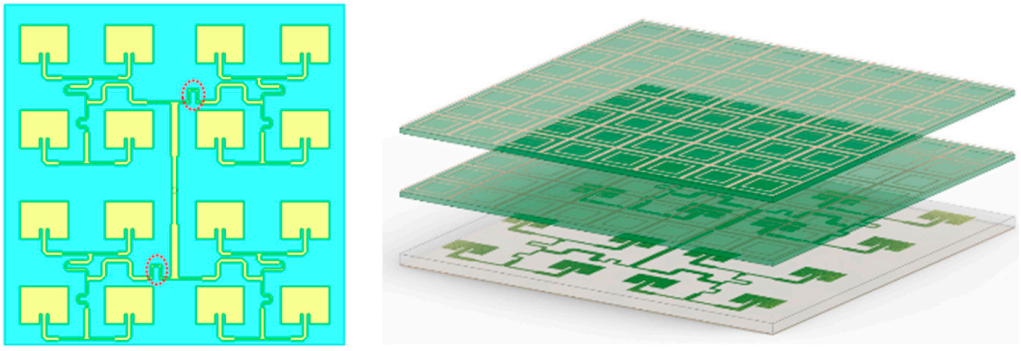

Figure 7. Antenna structure. (**a**) Reference; (**b**) design.

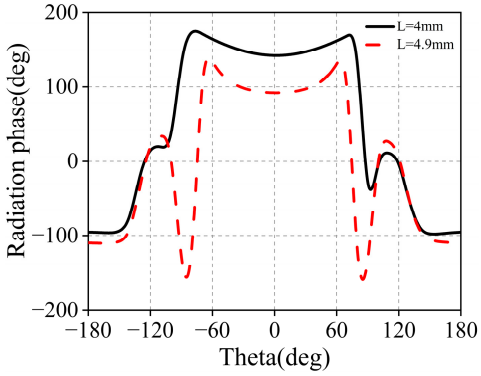

Figure 8. Radiation phases of metasurfaces of different sizes at 9.65 GHz.

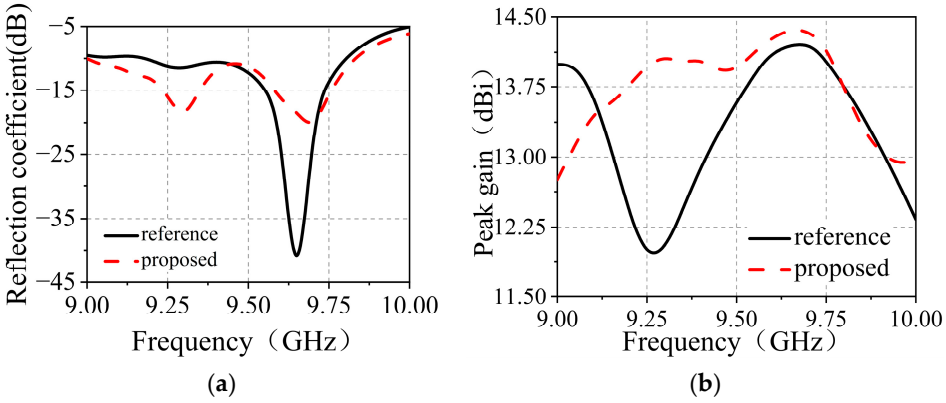

Figure 9. Designed antenna and reference antenna radiation performance. (**a**) Reflection coefficient; (**b**) peak gain.

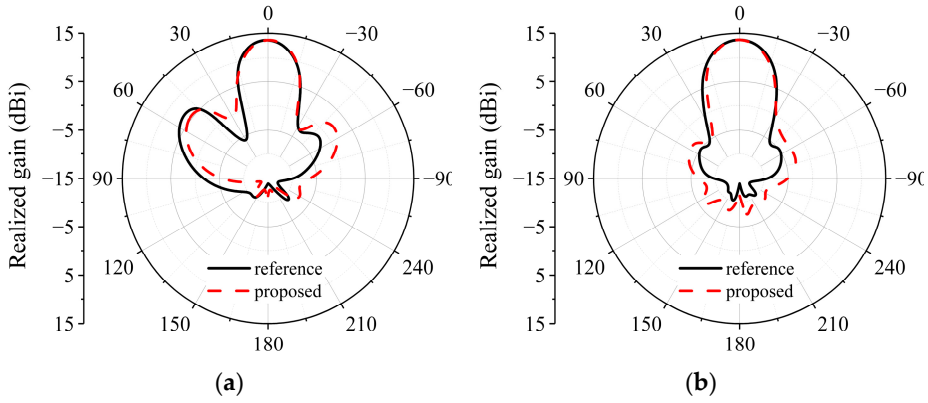

Figure 10. Radiation pattern of reference antenna and designed antenna at 9.65 GHz. (**a**) phi = 0°; (**b**) phi = 90°.

The monostatic RCS simulation results of the design and reference antenna are given in Figure 11. When the x-polarized plane wave is incident, compared with the reference antenna, the designed antenna exhibits varying degrees of RCS reduction in the entire operating frequency band. The proposed antenna achieves an in-band minimum RCS value of −28.9 dBsm at 9.25 GHz, resulting in a 12.31 dB reduction compared to the reference antenna. The average RCS reduction in the antenna within the operating frequency band exceeds 10 dB. When the y-polarized plane wave is incident, the proposed antenna attains an in-band minimum RCS value of −18.31 dBsm at 9.2 GHz, enabling a 10.91 dB reduction compared to the reference antenna. Moreover, the average RCS reduction in the antenna within the operating frequency band surpasses 9.1 dB. In Figures 12 and 13, the bistatic

RCS is plotted. It can be seen that the low observability can be found around the backward direction for the normally incident waves.

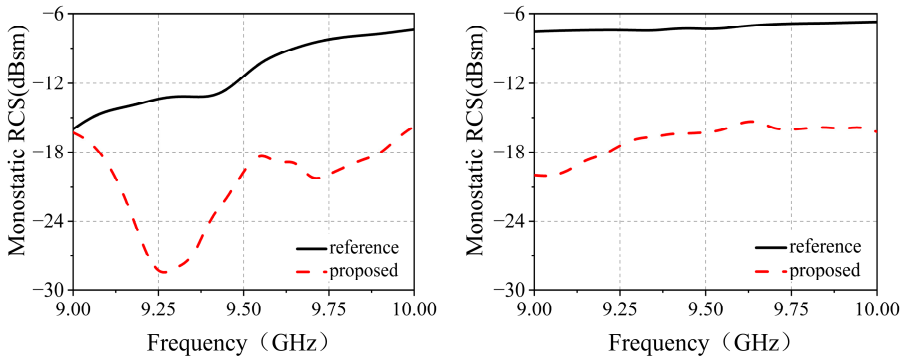

Figure 11. Monostatic RCS of the designed antenna and reference antenna. (**a**) x-polarization; (**b**) y-polarization.

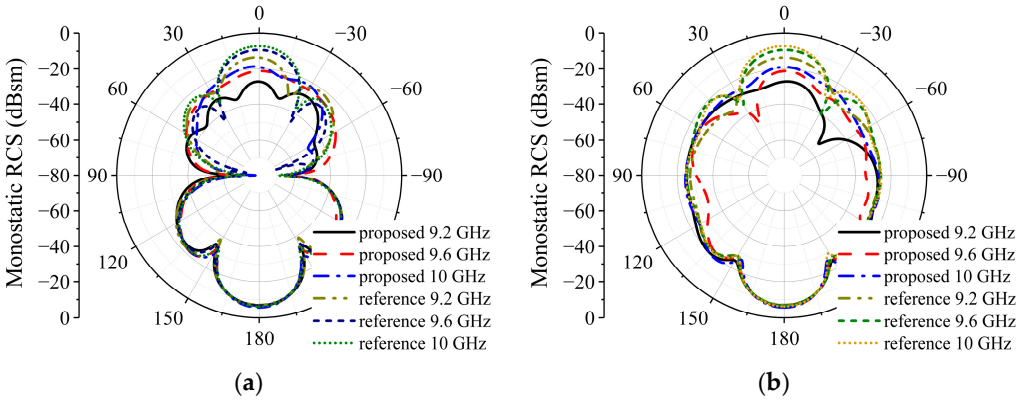

Figure 12. (**a**) Bistatic RCS pattern for co-pol normally incident waves in the (**a**) E- and (**b**) H-planes.

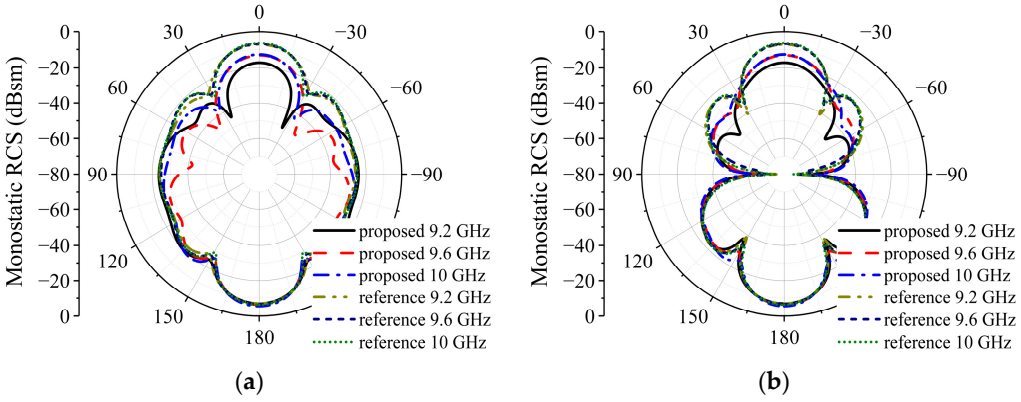

Figure 13. (**a**) Bistatic RCS pattern for cross-pol normally incident waves in the (**a**) E- and (**b**) H-planes.

3. Measured Result and Analysis

In order to verify the accuracy of the simulation results, the designed antenna was processed and tested, as shown in Figure 14. Figure 15 compares the simulation and test results of the designed low-RCS array antenna's radiation performance. It can be seen from Figure 15a that there is a frequency offset between the test results and the simulation results. Figure 15b is the peak gain comparison chart. Compared with the simulation, the test results are reduced by 0.21 dB at the frequency point of 9.65 GHz. The deviation of

the radiation performance is due to the fact that the metasurface and the patch antenna are separated by a gasket, and the air layer between them cannot be kept consistent with the simulation distance parameters, resulting in processing and assembly errors. Figure 16 depicts the measured and simulated radiation patterns, which align closely, validating the accuracy of the simulation results. The curves tend to be consistent, which verifies the accuracy of the simulation results. Table 1 gives a comprehensive comparison of the designed antennas and the antennas in the reference. By comparison, the antenna designed in this paper has the advantages of small size, large reduction value, and low loss.

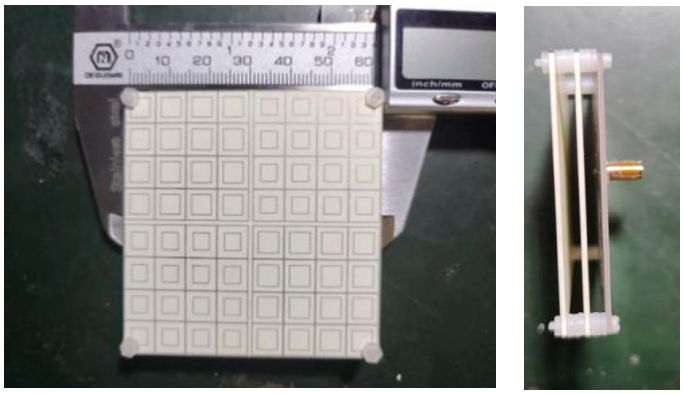

(**a**) (**b**)

Figure 14. Photographs of the proposed antenna. (**a**) Top view. (**b**) Side view.

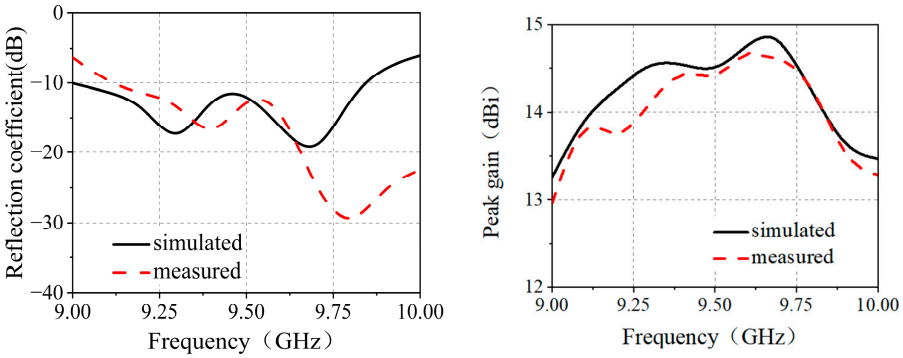

(**a**) (**b**)

Figure 15. Simulated and measured (**a**) reflection coefficient and (**b**) peak gain.

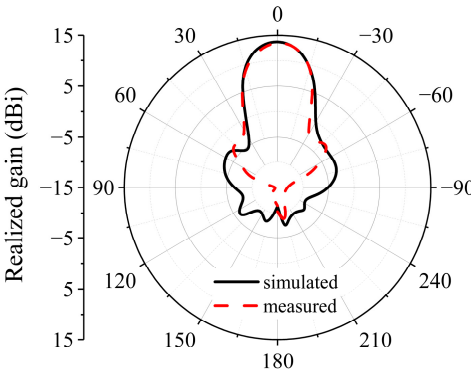

Figure 16. Radiation patterns at 9.65 GHz of the proposed antenna in the H-plane.

Table 1. Performance comparison with references.

Reference	Number of Units	Antenna Size (mm)	In-Band Co-Polarized RCS Reduction	Cross-Polarized Reduced Band (GHz)	Gain Drop (dB)
[7]	2×2	$1.08\lambda_0$	×	5.8–21.5	0.7
[9]	8×8	$4.56\lambda_0$	×	4.45–6.39, 11.94–15.87	0.3
[11]	4×4	$1.85\lambda_0$	×	2–4.1, 5.1–5.9	-
[12]	2×2	$1.8\lambda_0$	×	5.5–16.3	0.7
Proposed	4×4	$1.96\lambda_0$	√	9–10	0

4. Conclusions

An in-band low-RCS microstrip patch antenna based on a phase control metasurface is proposed in this paper. The average RCS reductions in co-polarization and cross-polarization in the operating frequency band are 10 dB and 9.1 dB, respectively. Moreover, the radiation performance of the antenna remains unaffected. Furthermore, the measured and simulated results show good agreement.

Author Contributions: Conceptualization, F.L.; methodology, F.L. and M.L.; software, F.L. and Y.J.; validation, M.L.; formal analysis, F.L., M.L., M.W. and Y.J.; investigation, M.W. and Y.J.; resources, M.W. and Y.J.; data curation, M.W. and Y.J.; writing—original draft preparation, F.L. and M.L.; writing—review and editing, F.L., M.L., M.W. and Y.J. All authors have read and agreed to the published version of the manuscript.

Funding: This research received no external funding.

Institutional Review Board Statement: Not applicable.

Informed Consent Statement: Not applicable.

Data Availability Statement: The data presented in this study are available on request from the corresponding author.

Conflicts of Interest: The authors declare no conflicts of interest.

References

1. Dikmen, C.M.; Çimen, S.; Çakır, G. Planar Octagonal-Shaped UWB Antenna With Reduced Radar Cross Section. *IEEE Trans. Antennas Propag.* **2014**, *62*, 2946–2953. [CrossRef]
2. Jiang, W.; Hong, T.; Liu, Y.; Gong, S.-X.; Guan, Y.; Cui, S. A Novel Technique for Radar Cross Section Reduction of Printed Antennas. *J. Electromagn. Waves Appl.* **2010**, *24*, 51–60. [CrossRef]
3. Ren, J.; Gong, S.; Jiang, W. Low-RCS Monopolar Patch Antenna Based on a Dual-Ring Metamaterial Absorber. *IEEE Antennas Wirel. Propag. Lett.* **2018**, *17*, 102–105. [CrossRef]
4. Ren, J.; Jiang, W.; Zhang, K.; Gong, S. A High-Gain Circularly Polarized Fabry–Perot Antenna With Wideband Low-RCS Property. *IEEE Antennas Wirel. Propag. Lett.* **2018**, *17*, 853–856. [CrossRef]
5. Sun, T.; Yin, F.; Xu, C.; Zhao, S.; Yan, H.; Yi, H. Ultrawideband Precision RCS Regulation for Trihedral Corner Reflectors by Loading Resistive Film Absorbers. *Electronics* **2022**, *11*, 3696. [CrossRef]
6. Zheng, Y.; Gao, J.; Cao, X.; Yuan, Z.; Yang, H. Wideband RCS Reduction of a Microstrip Antenna Using Artificial Magnetic Conductor Structures. *IEEE Antennas Wirel. Propag. Lett.* **2015**, *14*, 1582–1585. [CrossRef]
7. Xi, Y.; Jiang, W.; Wei, K.; Hong, T.; Cheng, T.; Gong, S. Wideband RCS Reduction of Microstrip Antenna Array Using Coding Metasurface With Low Q Resonators and Fast Optimization Method. *IEEE Antennas Wirel. Propag. Lett.* **2022**, *21*, 656–660. [CrossRef]
8. Zhou, Y.; Cao, X.; Gao, J.; Li, S.; Zheng, Y. In-Band RCS Reduction and Gain Enhancement of a Dual-Band PRMS-Antenna. *IEEE Antennas Wirel. Propag. Lett.* **2017**, *16*, 2716–2720. [CrossRef]
9. Li, M.; Shen, Z. Integrated Diffusive Antenna Array of Low Backscattering. *IEEE Antennas Wirel. Propag. Lett.* **2024**, *23*, 573–577. [CrossRef]
10. Genovesi, S.; Costa, F.; Monorchio, A. Wideband Radar Cross Section Reduction of Slot Antennas Arrays. *IEEE Trans. Antennas Propag.* **2014**, *62*, 163–173. [CrossRef]

11. Han, Y.; Zhu, L.; Bo, Y.; Che, W.; Li, B. Novel Low-RCS Circularly Polarized Antenna Arrays via Frequency-Selective Absorber. *IEEE Trans. Antennas Propag.* **2020**, *68*, 287–296. [CrossRef]
12. Chen, Q.; Guo, M.; Sang, D.; Sun, Z.; Fu, Y. RCS Reduction of Patch Array Antenna Using Anisotropic Resistive Metasurface. *IEEE Antennas Wirel. Propag. Lett.* **2019**, *18*, 1223–1227. [CrossRef]